www.springer.com/41230
https://doi.org/10.1007/s41230-023-2117-3
Research & Development
Vol. 20 No. 5 September 2023
CHINA FOUNDRY

Influence of heat treatments on incipient melting structures of DD5 nickel-based single crystal superalloy

*Zhi-hong Jia, Chen-yang Li, Wen-xiang Jing, Xiang-feng Liang, Ze-kun Zhang, Jia-le Xiao, and Yu-tao Zhao
School of Materials Science and Engineering, Jiangsu University, Zhenjiang 212013, Jiangsu, China

Abstract: The evolution of microstructure and formation mechanism of incipient melting microstructure of DD5 single crystal superalloy during solution heat treatment were studied by scanning electron microscopy (SEM), electron probe microanalysis (EPMA), and energy dispersive spectroscopy (EDS). The solidus and liquidus of single crystal alloy were obtained by differential scanning calorimetry (DSC). Results show that the mosaic-like eutectic and fan-like eutectic are dissolved at first, and the coarse γ' phase is dissolved later during the solution heat treatment of 1,390 °C/2 h+1,310 °C/4 h+1,320 °C/10 h + air cooling (AC). The composition segregations of Al, Ta, W and Re are 0.99, 0.96, 1.04 and 1.16, respectively, which close to 1. The incipient melting is caused by the low local temperature of the alloy, and the micropore region with a lower melting point is the preferred position for incipient melting.

Keywords: superalloy; solution heat treatment; eutectic; composition segregation; incipient melting

CLC numbers: TG146.1+5 **Document code:** A **Article ID:** 1672-6421(2023)05-395-08

1 Introduction

Nickel-based single crystal (SC) superalloys have been widely used in aero-engine turbine blades due to their excellent high temperature mechanical properties [1-4]. To improve the mechanical properties of the SC superalloy, numerous refractory elements are added, while the composition segregation of the alloy also increases significantly [5]. The second generation SC superalloy can effectively strengthen the small angle grain boundary of the alloy by adding a small amount of C, B and Hf [6]. However, the research results show that the addition of trace elements will decrease the local temperature of the alloy, thus leading to the local incipient melting [7-9]. The homogenization process below the dissolution temperature of γ' phase is considered to be an effective method to avoid the incipient melting, and the highest solution temperature of the alloy can be effectively increased by a reasonable pretreatment process [10].

The incipient melting is the most challenging part in the design of solid solution heat treatment due to the low temperature of local solid solution. Micropores and recrystallization occur during incipient melting, which deteriorates mechanical properties at high temperature [11]. Micropores and eutectic morphologies are often used to determine the microstructure characteristics of incipient melting [12-14]. Hegde et al. [15] found that long-term isotherm kept above the equilibrium solid temperature will cause upward diffusion of the eutectic zone. Then, the incipient melting comes up. Wang et al. [16] tested the tensile properties of CMSX-4 alloy and found that most of the cracks are caused by micropores. Besides, the larger the size of the pore, the earlier the crack occurs, and the faster the crack propagation rate. Currently, many studies have been carried out on the eutectic structure and porosity of superalloy after solid solution heat treatment [17-19]. Nevertheless, there are few systematic studies conducted on the incipient melting structure, let alone the comparative study on the micropores formed after solid solution heat treatment and the incipient melting pores. Therefore, it is of great significance to study the formation law of incipient melting structure, so as to avoid incipient melting and improve the properties of SC superalloy.

In this study, the incipient melting and micropores of DD5 SC superalloy after solution treatment were systematically studied, and the mechanism of the dissolution of eutectic phase and the formation of the incipient melting were elucidated. Finally, the solid solution heat treatment process for completely

***Zhi-hong Jia**
Born in 1976, Ph. D., Associate Professor. His research interests mainly focus on superalloy, Al alloy, Cu alloy, and their casting processes.
E-mail: jia_zh@ujs.edu.cn
Received: 2022-09-02; Accepted: 2023-03-21

eliminating eutectic and incipient melting was developed, aiming at providing a reference for the application of the SC superalloys.

2 Experimental

DD5 alloy, with nominal composition of Ni-6.2Al-7.5Co-7.0Cr-0.15Hf-1.5Mo-3Re-6.5Ta-5W-0.043C-0.078Y-0.041B (wt.%) was employed. A rod sample with a diameter of 20 mm and a height of 160 mm was prepared by using a VDF-10 vacuum induction directional solidification furnace with a withdrawing rate of 3 mm·min^{-1}. The rod was cut into several cylindrical samples with a height of 5 mm by wire cutting along the growth direction of single crystal ([001]).

Metallographic samples were chemically etched with a 1:1 mixture of 30% hydrogen peroxide and 36% hydrochloric acid. A JXA-8530F Plus field emission electron probe (EPMA) was used to detect the element distribution at the incipient melting position of the alloy. Image-Pro Plus was used to calculate the eutectic phase content of the heat-treated alloy and the area and volume fractions of the incipient melting pores and micropores. At least 15 locations were selected for calculating the average value.

The DSC curves of the alloy were obtained through thermal differential analysis to confirm the heat treatment interval. A STA 449 F3 synchronous thermal analyzer was used, and the heating rate of the alloy was 20 °C·min^{-1} below 800 °C and 10 °C·min^{-1} above 800 °C. After heated to 1,500 °C, it was cooled to 800 °C and finally cooled to room temperature.

Figure 1 shows the DSC results of the as-cast alloy. Three absorption peaks are found in this process. The first absorption peak (1,294.4 °C) is the resolution temperature of γ' phase, the second one (1,306.4 °C) is the temperature at which eutectic phase begins to be dissolved, and the third one (1,350.7 °C) is the liquidus of single crystal alloy. According to the tangent method, the solidus of the alloy is 1,330.9 °C, so the heat treatment interval is preliminarily set as 1,290 °C–1,330 °C.

A single stage of heat treatment at 1,310 °C for 2 h was carried out to further confirm the incipient melting temperature range. The multi-stage solution heat treatment temperature range was 1,315 °C–1,325 °C based on the single-stage solution heat treatment [19-20].

Before the stepwise solution heat treatment experiment, a pretreatment experiment was designed, which was holding at 1,290 °C for 2 h, aiming to stabilize the eutectic phase and increase the incipient melting temperature of the alloy. After many solid solution treatment experiments, four stepwise solid solution heat treatment processes, as shown in Table 1, were finally designed to study the dissolution kinetics of the eutectic phase in the solid solution treatment process. The highest solution treatment temperature of SSHT1 was 1,315 °C, and that of SSHT2 was 1,320 °C. To study the effect of holding time on the microstructure and homogenization of the alloy, SSHT3 was held for 4 h more than SSHT2 in the high temperature solution section (1,320 °C), and to study the effect of different temperatures on the microstructure and homogenization of the alloy, the highest solution treatment temperature of SSHT4 was increased to 1,325 °C. The heating furnace was the SX-1700C box furnace, and air cooling was used.

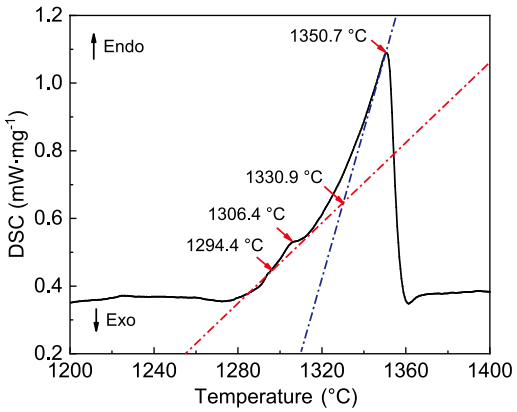

Fig. 1: DSC curves of DD5 single crystal alloy

Table 1: Stepwise solution heat treatment processes

Experiment	Solution heat treatment	Duration
SSHT1	1,290 °C/2 h+1,310 °C/4 h+1,315 °C/6 h, AC	12 h
SSHT2	1,290 °C/2 h+1,310 °C/4 h+1,320 °C/6 h, AC	12 h
SSHT3	1,290 °C/2 h+1,310 °C/4 h+1,320 °C/10 h, AC	16 h
SSHT4	1,290 °C/2 h+1,310 °C/4 h+1,325 °C/10 h, AC	16 h

3 Results and discussion

3.1 Composition segregation

Figure 2(a) shows the morphology of γ/γ' eutectic structure in the as-cast state. Li et al. [17] divided the eutectic structure into three types according to different solidification sequences: mosaic-like eutectic, fan-like eutectic, and coarse γ' phase. Figure 2(b) shows the microstructure of the sample after a single stage treatment at 1,310 °C for 2 h. It can be seen, after a single stage of heat treatment, the fine mosaic-like eutectic is completely dissolved, however the fan-like eutectic is too big to be completely dissolved. The fan-like eutectic phases that are not completely dissolved differ greatly in grain size. A few of them grow preferentially and absorb the surrounding fine

grains, consequently, the coarse eutectic phase is formed, as shown in Fig. 2(b). Figure 2(c) shows the microstructure of the sample after SSHT2 treatment. In the interdendritic region, there are still some coarse γ' phases that are not completely dissolved. However, by using stepwise solution heat treatments and increasing the total solid solution time, eutectic phase in Fig. 2(b) disappears. Furthermore, the incipient melting pore is formed near the coarse γ' phase. Figure 2(d) shows the microstructure of the sample after SSHT3 treatment. It can be seen that the γ/γ' eutectic phase is completely dissolved, only the fine γ' phase re-precipitated after air cooling is remained.

Figure 3 indicates the SEM microstructures of alloy samples after different solution heat treatment processes. In Fig. 3(a), it can be seen there are still some residual eutectics in the SSHT1 sample, the eutectic content is 4.4%, and thick γ' phase is found in the matrix. The eutectic phase in the SSHT2 sample is only 1.4%, far less than the SSHT1 sample, as shown in Fig. 3(b); and when partial dissolution of the coarse γ' phase occurs, a small amount of circular incipient melting appears in the interdendritic region [red circle in Fig. 3(b)]. For the SSHT3

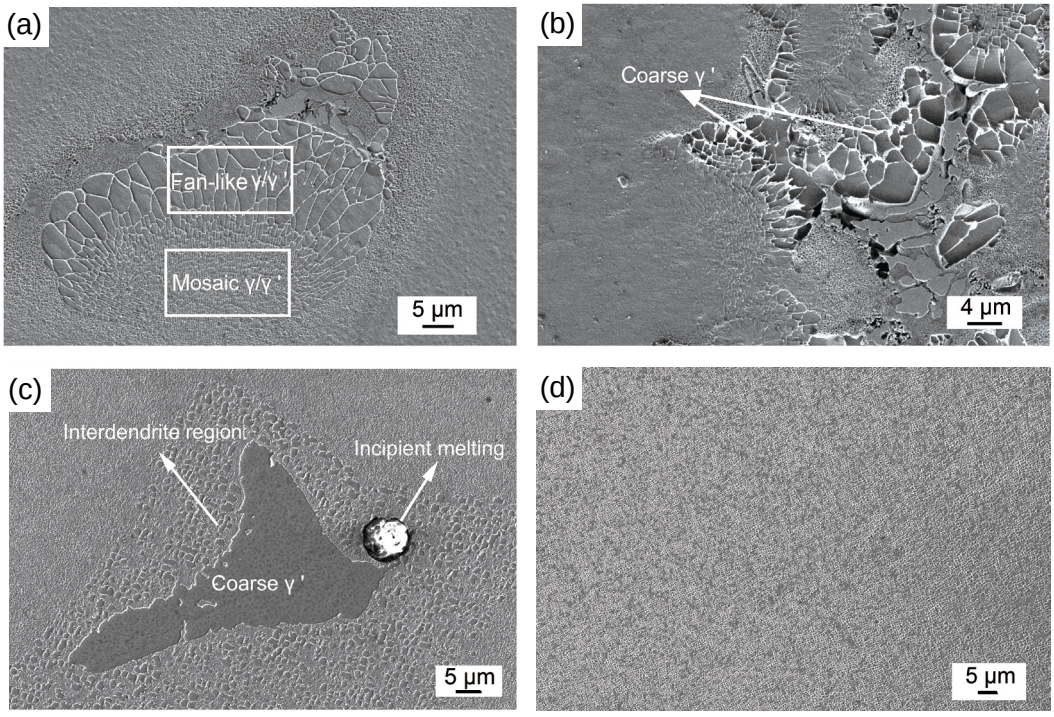

Fig. 2: Dissolution process of eutectic of the alloy at different states: (a) as-cast; (b) 1,310 °C/2 h; (c) SSHT2; (d) SSHT3

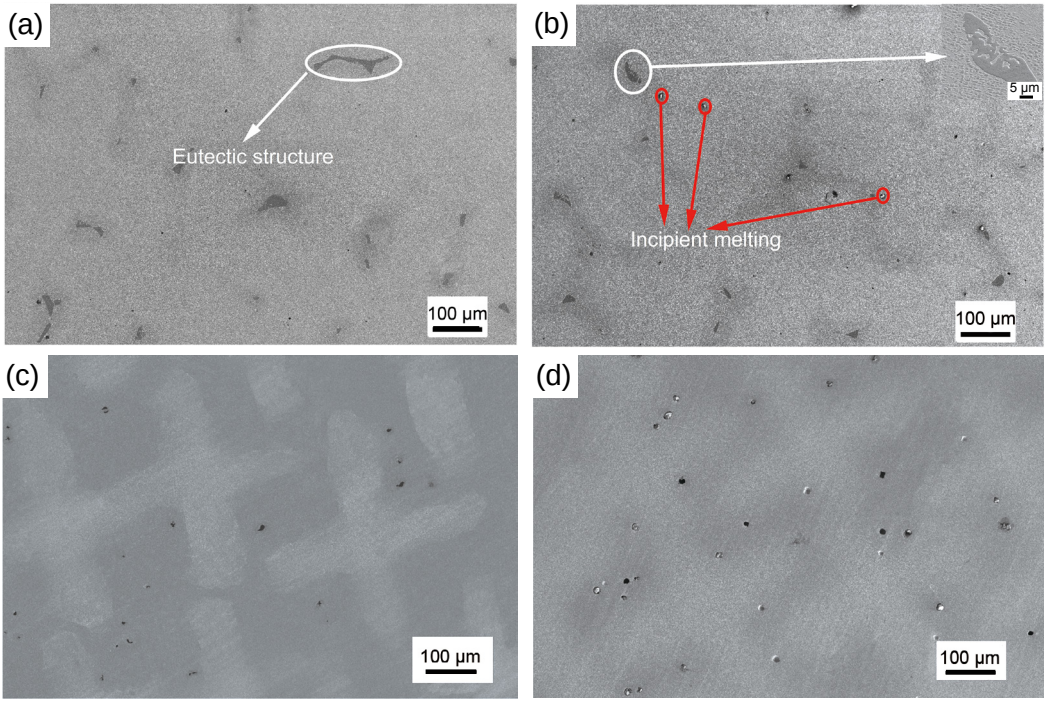

Fig. 3: SEM images of alloy samples treated with different solution treatments: (a) SSHT1; (b) SSHT2; (c) SSHT3; (d) SSHT4

sample, with a 4 h longer holding time at the high temperature (1,320 °C), the γ/γ' eutectic microstructure is almost completely dissolved, and no incipient melting is found [Fig. 3(c)]. While, as the solution temperature rises to 1,325 °C, numerous incipient melting microstructures appear in the SSHT3 alloy [Fig. 3(d)]. This is because when the solution temperature increases to 1,325 °C, the heating rate is too fast (5 °C·min^{-1}), which is much greater than the incipient melting nucleation rate of the alloy [21]. Therefore, it can be concluded that properly extending of the holding time at the highest solution temperature is conducive to the homogenization of the alloy and the dissolution of the eutectic phase, hence the incipient melting phenomenon caused by a too low local temperature can be avoided.

To further understand the segregation degree of alloy elements before and after heat treatment, the segregation coefficient K_i is defined as:

$$K_i = C^i_{\text{dendrite}} / C^i_{\text{interdendrite}} \quad (3)$$

which represents the degree of segregation between dendritic core and interdendrite. C^i_{dendrite} and $C^i_{\text{interdendrite}}$ represent the element concentration of element *i* in the dendritic core regions and interdendritic regions, respectively.

The composition segregation of the alloy as cast and under different heat treatments is shown in Table 2 and Fig. 4. It can be seen from Table 2 that there is serious composition segregation in the as-cast alloy, Co, Cr, Re and W are segregated in dendritic core, especially the refractory elements Re and W. The segregation coefficient of Re in as-cast alloy is 4.12, while that of W is 2.58. Aluminum (Al), Mo and Ta are segregated in the interdendrite, and the segregation of Al and Ta is more serious than Mo. Their segregation coefficients are 0.64 and 0.17, respectively. After the solution treatment of SSHT1, the segregation of the alloy is improved. The segregation coefficient of insoluble element W and Re is close to 1.5 and 2, and that of Al and Ta is 0.78 and 0.61. When the maximum solution temperature is increased to 1,320 °C and holding for 6 h, the segregation of all the elements in the alloy is further improved (SSHT2). When the holding time at the highest solution temperature (1,320 °C) is extended to 10 h, the segregation is obviously improved, and the segregation coefficients of Al, Ta, W and Re are 0.99, 0.96, 1.04 and 1.16, respectively (SSHT3), which close to 1. Further increasing the temperature does not significantly improve the segregation, but leads to the incipient melting of the alloy (SSHT4), as shown in Fig. 3. For all the samples, change of the segregation coefficient of Mo is not obvious, stabilized at about 0.80, due to that the Mo content is far lower than other elements. Studies show that due to the small diffusion coefficients of W and Re, they need a higher solution temperature and a longer holding time to be homogenized [7,15,22,23]. However, a too high solution temperature will cause the incipient melting of the alloy, and a longer holding time will increase the cost of heat treatment.

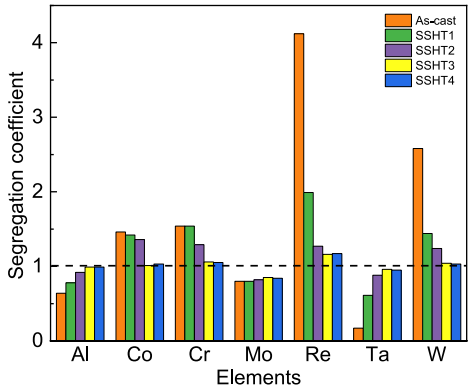

Fig. 4: Composition segregation of samples in as-cast state and different solution treatments

Table 2: Composition segregation of specimens (wt.%)

State	Location	Composition							
		Al	Co	Cr	Mo	Re	Ta	W	Ni
As-cast	Dendritic core	5.14	7.80	8.05	1.67	7.37	0.72	9.27	59.60
	Interdendrite	8.03	5.33	5.23	2.08	1.79	4.16	3.59	64.49
	K_i	0.64	1.46	1.54	0.80	4.12	0.17	2.58	0.92
SSHT1	Dendritic core	5.35	12.52	8.22	1.42	1.73	2.42	8.79	59.25
	Interdendrite	6.86	8.82	5.34	1.77	0.87	3.94	6.10	62.73
	K_i	0.78	1.42	1.54	0.80	1.99	0.61	1.44	0.94
SSHT2	Dendritic core	5.27	11.69	5.83	0.73	1.50	2.14	8.51	60.10
	Interdendrite	5.73	8.60	4.53	0.89	1.18	2.42	6.86	62.87
	K_i	0.92	1.36	1.29	0.82	1.27	0.88	1.24	0.96
SSHT3	Dendritic core	5.26	11.97	5.37	0.46	1.60	1.36	7.30	63.99
	Interdendrite	5.32	11.83	5.07	0.54	1.38	1.41	7.05	64.48
	K_i	0.99	1.01	1.06	0.85	1.16	0.96	1.04	0.99
SSHT4	Dendritic core	5.72	11.26	4.78	0.54	1.61	2.01	7.14	63.41
	Interdendrite	5.79	10.94	4.54	0.64	1.38	2.11	6.96	63.88
	K_i	0.99	1.03	1.05	0.84	1.17	0.95	1.03	0.99

3.2 Solution treatment and composition segregation

Figures 5 and 6 demonstrate the morphology of micropores and incipient melting pores of the samples after different solution treatment processes, respectively. The number, size and area ratio of incipient melting and micropores after different solution treatments are shown in Table 3. After SSHT1 treatment, there is no obvious incipient melting in the microstructure of the sample, and the edge of the micropore is serrated. The γ' phase near the micropore is partially dissolved, and the γ' phase far away from the micropore is regular in shape and uniformly distributed [Fig. 5(a)]. When the maximum solution treatment temperature rises to 1,320 °C, the γ' phase at the edge of the micropore starts to melt [the red dotted line in Fig. 5(b)], and the micropore's morphology changes from round to irregular ellipse. The average area of the micropores also expands from 3.81 μm^2 to 15.80 μm^2 (Table 3), this phenomenon confirms that the dissolution of γ' phase at the edge of the micropores is preferred in the solution treatment. Figures 5(c) and (d) show the micropore morphology of SSHT3 samples. With the extension of holding time, the number of micropores is decreased (Table 3), but the average pore area is gradually increased to 52.22 μm^2. When the highest solution temperature further rises to 1,325 °C (SSHT4), the γ′ phase at the edge of micropores becomes regular, and the micropore area is continuously increased to 68.21 μm^2.

Because most of the micropores are located in the vicinity of γ/γ′ eutectic phase and interdendritic region, there is serious dendritic segregation in the as-cast microstructure. The γ′ phase-forming elements such as Al and Ta segregate in the interdendritic regions and the refractory elements such as W and Re segregate in the dendritic core (Table 2). Compared with W and Re, elements Al and Ta have a lower melting point, especially Al (660 °C). As a result, the melting point of the phase in the interdendritic region is generally lower than that of the dendritic core, so, the incipient melting is more prone to occur in the interdendrite. It can be seen from Figs. 6(a)–(d) that the incipient melting pore has a similar morphology to the micro-

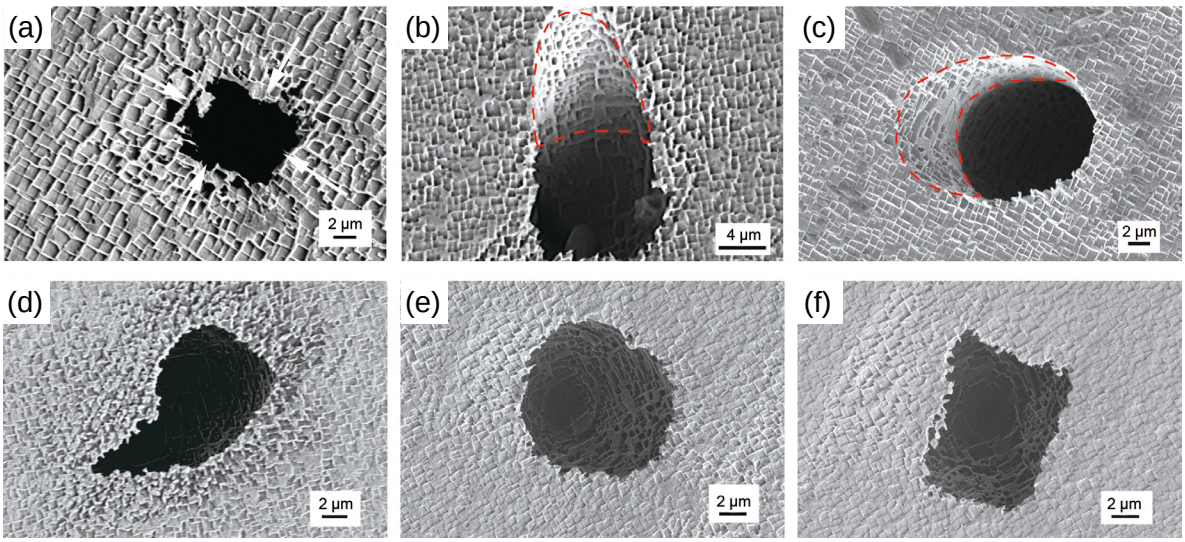

Fig. 5: SEM images of micro-pores after different solution treatments: (a) SSHT1; (b) SSHT2; (c) and (d) SSHT3; (e) and (f) SSHT4

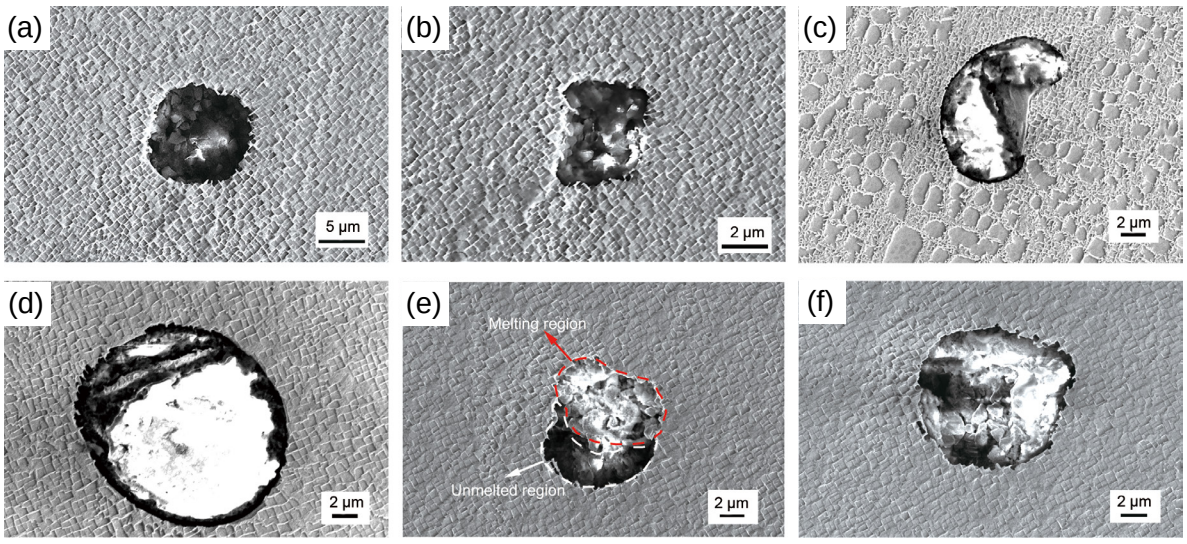

Fig. 6: SEM images of incipient melting pores after different solution treatments: (a, b, c) SSHT2; (d, e, f) SSHT4

Table 3: Change of micropores and incipient melting after different heat treatments

Treatment	Type of pores	No.	Area (μm²)			Porosity (%)	Sum of porosity
			Max	Min	Mean		
SSHT1	Micropores	39	22.81	0.79	3.81	0.017	0.017
SSHT2	Micropores	30	69.26	0.79	15.80	0.071	0.133
	Incipient melting	9	110.18	11.02	75.44	0.062	
SSHT3	Micropores	22	97.59	3.15	52.22	0.093	0.093
SSHT4	Micropores	9	133.00	18.89	68.21	0.071	0.261
	Incipient melting	14	212.49	55.88	148.64	0.190	

pores. Melt-like substances are precipitated out of the incipient melting pore, and the intermediate area shows bright white under scanning electron microscopy (SEM) [Figs. 6(c) and (d)]. However, the micropores are a hollow structure, while the incipient melting pores are mostly round. It can be seen from Fig. 6(e) that incipient melting occurs in the red dotted line area, and the white dotted line area is still in a hollow state, indicating that the micropores have not been completely melted. This phenomenon further indicates that the micropore's region with a lower melting point is preferable for incipient melting.

In the case of the same solid solution time, the increase of solid solution temperature will lead to the increase of the size of micropores and incipient melting pores and porosity. As shown in Table 3, when the highest solution temperature increases from 1,315 °C to 1,320 °C, the porosity of the alloy increases from 0.017% of SSHT1 to 0.071% of SSHT2. However, as the solution temperature increases from 1,320 °C to 1,325 °C, the porosity decreases from 0.093% of SSHT3 to 0.071% of SSHT4. When the solution temperature reaches 1,325 °C, the γ' phase at the edge of the micropores will dissolve at first (local temperature is low). As a result, the micropore area will become larger. When the temperature rises to the critical solid solution temperature, the larger micropores are more prone to incipient melting than smaller ones [16]. The incipient melting is caused by the low local temperature of the alloy [21], so the micropore area with a lower melting point is the preferred position for the incipient melting. During the solution treatment stage, some large micropores with lower melting points will preferentially undergo incipient melting, so the area of these incipient melting pores is generally greater than that of micropores, resulting in convex melt-like substances on the surface of the alloy. This part of the incipient melting converted from micropores is not included in the porosity in Table 3, therefore, the porosity of the above-mentioned SSHT4 is less than that of SSHT3. Also, it can be found that the porosity of incipient melting + micropores increases with the increase of solid solution temperature under the same solid solution time (compare SSHT1 and SSHT2 or SSHT3 and SSHT4).

EDS was carried out to comparatively analyze the elements in the area of micropores and incipient melting pores. Fifteen micropores and 15 incipient melting pores in the same area of the same sample were selected for surface scanning analysis, and the average value of the 15 measurements was taken as the result. As shown in Fig. 7, the content of Ta in the incipient melting position is much higher and that of W and Ni is much lower than that of the micropore region, while the segregation of other elements is not obvious. With the increase of the solution temperature, the γ/γ' eutectic structure dissolves, Al and Ta elements diffuse into the dendritic core region, Re and W elements diffuse into the interdendritic region (Table 2), thus reducing the segregation degree of the alloy. When the solution treatment temperature is higher than the local low melting point, incipient melting will form in this area (a large micropore area). Due to the high content of Ta element (melting point 2,996 °C) and the low content of W element (melting point 3,620 °C), the overall melting point of the γ′ phase at the edge of the micropores in the interdendritic region will be lower than that of other positions, and thus the incipient melting will be preferentially formed during the solution treatment process. Another γ′ phase forming element Al has a faster diffusion rate and a smaller segregation during the solution treatment process, so its segregation in the micropores and incipient melting pores is not obvious.

To further compare the element distribution of the incipient melting area, a more accurate EPMA was employed for surface scanning of the incipient melting location, and the results are shown in Fig. 8. The content of Al element is higher in the middle area of the incipient melting, but less in the edge. The

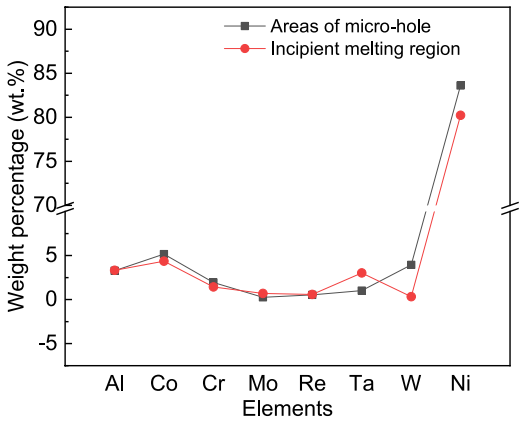

Fig. 7: Composition comparison of the incipient melting and micropores

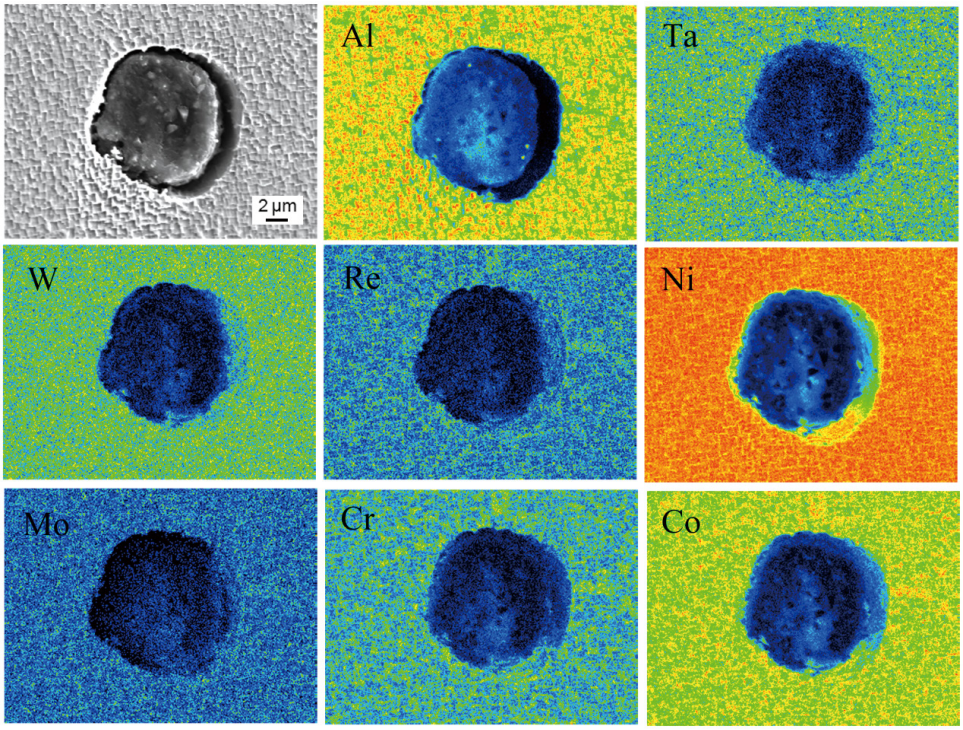

Fig. 8: EPMA maps of incipient melting area

edge of the incipient melting pore is rich in Ta, W, Re, Ni and the other elements. The area around the incipient melting pore contains a large amount of Al, Co, Ni and the other elements with a low melting point, which leads to the melting point of this area lower than that of other areas.

4 Conclusions

(1) In the process of heat treatment, the surrounding fine grains would be absorbed by partial fan-like eutectic phase which is not completely dissolved, thus resulting in the grains growing abnormally and forming of the coarse γ' phase. After 1,310 °C/2 h, the mosaic-like eutectics and the fan-like eutectics are dissolved, and all the eutectics completely dissolved after SSHT3 treatment.

(2) Under the premise of no incipient melting of the sample, the element segregation after SSHT3 treatment is obviously improved. The composition segregation of Al, Ta, W and Re reaches 0.99, 0.96, 1.04 and 1.16, respectively, which close to 1.

(3) During solution heat treatment, the γ' phase at the edge of the micropores are melted at first, leading to the expansion of the area of the micropores. The large-area micropores locate in the zone with a low local temperature, and the incipient melting is caused by the low local temperature of the alloy, thus, the large-area micropores are easier to form incipient melting.

(4) When the solution temperature rises, both the micropore size and the incipient melting pore size are enlarged. At the same solution temperature, the micropore size of the alloy will expand if the holding time is lengthened. Moreover, when the solution temperature rises, the smaller micropores will be filled up by the surrounding γ' phase, bringing a decrease in the number of micropores.

Acknowledgement

The authors would like to express their sincere thanks to the financial support from the Key Project of National Natural Science Foundation of China (No. U16642548).

Conflict of interest

The authors declare that they have no known competing financial interests or personal relationships that could have appeared to influence the work reported in this paper.

References

[1] Yang W, Li J, Liu S, et al. Orientation dependence of transverse tensile properties of nickel-based third generation single crystal superalloy DD9 from 760 to 1100 °C. Transactions of Nonferrous Metals Society of China, 2019, 29(3): 558−568.
[2] Paraschiv A, Matache G, Puscasu C. The effect of heat treatment on the homogenization of CMSX-4 single-crystal Ni-based superalloy. Transportation Research Procedia, 2018, 29: 303−311.
[3] Xu M, Geng X Q, Zhang X L, et al. Effect of competitive crystal growth on microstructural characteristics of directionally solidified nickel-based single crystal superalloy. Journal of Alloys and Compounds, China Foundry, 2022, 19(2): 109−116.
[4] Wang X D, Yang Z, Gao Q, et al. Effect of long-term thermal exposure on microstructure and creep properties of DD5 single crystal superalloy. China Foundry, 2021, 18(3): 185−191.
[5] Cui R, Huang Z. Microstructual evolution and stability of second generation single crystal nickel-based superalloy DD5. Transactions of Nonferrous Metals Society of China, 2016, 26(8): 2079−2085.
[6] Liu S, Shi Z, Li J. Effect of C content on microstructure of second generation single crystal superalloy. Journal of Aeronautical Materials, 2017, 37(3): 9−15.

[7] Zhang Y, Liu L, Huang T, et al. Investigation on remelting solution heat treatment for nickel-based single crystal superalloys. Scripta Materialia, 2017, 136: 74–77.
[8] Mostafaei M, Abbasi S M. Influence of Zr content on the incipient melting behavior and stress-rupture life of CM247 LC nickel base superalloy. Journal of Alloys and Compounds, 2015, 648: 1031–1037.
[9] Jahangiri M R, Boutorabi S M A, Arabi H. Study on incipient melting in cast Ni base IN939 superalloy during solution annealing and its effect on hot workability. Materials Science and Technology, 2012, 28(12): 1402–1413.
[10] Hegde S R, Kearsey R M, Beddoes J C. Designing homogenization – solution heat treatments for single crystal superalloys. Materials Science and Engineering: A, 2010, 527(21–22): 5528–5538.
[11] Mostafaei M, Abbasia S M, Mostafaei M A. Improvement of γ' coarsening model in high γ' volume fraction Ni-base superalloys containing different Ta/W ratio. Journal of Alloys and Compounds, 2021: 160938.
[12] Li X, Jia C, Zhang Y, et al. Incipient melting phase and its dissolution kinetics for a new superalloy. Transactions of Nonferrous Metals Society of China, 2020, 30(8): 2107–2118.
[13] Karunaratne M S A, Cox D C, Carter P, et al. Modelling of the microsegregation in CMSX-4 superalloy and its homogenisation during heat treatment. Superalloys, 2000: 263–272.
[14] Ojo O A, Richards N L, Chaturvedi M C. On incipient melting during high temperature heat treatment of cast Inconel 738 superalloy. Journal of Materials Science, 2004, 39(24): 7401–7404.
[15] Hegde S R, Kearsey R M, Beddoes J C. Designing homogenization-solution heat treatments for single crystal superalloys. Materials Science and Engineering: A, 2010, 527(21–22): 5528–5538.
[16] Wang H, Ning L K, Tong J, et al. Effect of heat treatment on microstructures and stress rupture properties in the nickel base single crystal superalloy CMSX-4. Rare Metal Materials and Engineering, 2020, 49(1): 247–256.
[17] Li X W, Wang C, Zhang Y Z, et al. Effect of nitrogen on micro-pores in DD33 single crystal superalloy during solidification and homogenization. China Foundry, 2022, 19(4): 281–287.
[18] Epishin A, Fedelich B, Link T, et al. Pore annihilation in a single-crystal nickel-base superalloy during hot isostatic pressing: Experiment and modelling. Materials Science and Engineering: A, 2013, 586: 342–349.
[19] Li Y S, Xuan W D, Yang J, et al. Evolution mechanism of recrystallization in a nickel-based single crystal superalloy under various cooling rates during heat treatment. China Foundry, 2022, 19(1): 27–34.
[20] Yang Y X, Wang Y, Liu G H, et al. Microstructure evolution and mechanical properties of DD6 single crystal superalloy during heat treatment process. Heat Treatment of Metals, 2022, 47(11): 1–11.
[21] Zhang Y B, Liu L, Huang T W, et al. Incipient melting and solution heat treatment of a boron-bearing third generation single crystal nickel base superalloy. Rare Metal Materials and Engineering, 2017, 46(10): 3105–3110.
[22] Bokstein B S, Epishin A I, Link T, et al. Model for the porosity growth in single-crystal nickel-base superalloys during homogenization. Scripta Materialia, 2007, 57(9): 801–804.
[23] Fuchs G E. Solution heat treatment response of a third generation single crystal Ni-base superalloy. Materials Science and Engineering: A, 2001, 300(1–2): 52–60.